Results in Physics 7 (2017) 57–68

Contents lists available at ScienceDirect

Results in Physics

journal homepage: www.journals.elsevier.com/results-in-physics

# MHD pulsatile flow of engine oil based carbon nanotubes between two concentric cylinders

Rizwan Ul Haq [a,*], Faisal Shahzad [b], Qasem M. Al-Mdallal [c]

[a] Department of Electrical Engineering, Bahria University, Islamabad Campus, Islamabad 44000, Pakistan
[b] Department of Mathematics, Capital University of Science and Technology, Islamabad 44000, Pakistan
[c] Department of Mathematical Sciences, UAE University, Al Ain, P.O. Box 15551, United Arab Emirates

ARTICLE INFO

*Article history:*
Received 7 October 2016
Received in revised form 23 November 2016
Accepted 25 November 2016
Available online 29 November 2016

*Keywords:*
MHD
Pulsating flow
Nanofluids
Carbon nanotubes
Concentric cylinders

ABSTRACT

In this article, thermal performance of engine oil in the presence of both single and multiple wall carbon nanotubes (SWCNTs and MWCNTs) between two concentric cylinders is presented. Flow is driven with oscillatory pressure gradient and magneto-hydrodynamics (MHDs) effects are also introduced to control the random motion of the nanoparticles. Arrived broad, it is perceived that the inclusion of nanoparticles increases the thermal conductivity of working fluid significantly for both turbulent and laminar regimes. Fundamental momentum and energy equations are based upon partial differential equations (PDEs) that contain thermos-physical properties of both SWCNTs and MWCNTs. The solution has been evaluated for each mixture, namely: SWCNT-engine oil and MWCNT-engine oil. Results are determined for each velocity, temperature, pressure and stress gradient. Graphical results for the numerical values of the emerging parameters, namely: Hartmann number ($M$), the solid volume fraction of the nanoparticles ($\phi$), Reynolds number ($Re_{\omega}$), and the pulsation parameter based on the periodic pressure gradient are analyzed for pressure difference, frictional forces, velocity profile, temperature profile, crux, streamlines and vorticity phenomena. In addition, the assets of various parameters on the flow quantities of observation are investigated.



## Introduction

The study of pulsatile flow has attained a considerable attention based on several investigations at industrial level. Flows in a conduit/cylinder brought about via sinusoidal influence in the waves transmitting alongside of the channel's walls are determined through pulsatile flows. The study of the fluids that reveal oscillatory flow have numerous important application in nature; common examples in medical sciences included blood flow through an artery, peristaltic food motion in the intestine and motion of urine in the urethra. Moreover, in astrophysics and geophysics, its miles implemented to the have a look at of stellar shape, cores terrestrial and sun plasma.

In the early stages, Atabek et al. [1] calculated the time dependent flow in tubular pipe and carried out the analytical results for variation of the velocity profile. After this concept, Vardanyan et al. [2] had developed several theoretical models on the influence of magnetic strength of pulsatile type flow. They had mentioned that in the presence of consistent and uniform magnetic strength leads to decrease the flow rate. In fact, their work has a significant impact on biological research. Richardson and Tyler [3,4] presented the experimental results in the existence of an important structure which deals with the oscillating flow that is known as annular effect. Subsequent studies of Womorsley [5] and Uchida [6] established these results by analyzing the sinusoidal motion that is dealing for incompressible oscillating fluid along a flat conduit. Apart from all above theoretical studies, the real world applications related to the present analysis are deal for various physical geometries as mentioned by various authors. Recently, Yang et al. [7] constructed optimization for whole cylinder with pin-fin heat sinks using the finite volume method (FVM). In their study, the maximum heat transfer rate is utilized as the objective to maintain total heat sink volume and fin-material volume, whereas the pressure drop is implemented to evaluate the hydraulic performance of the system. In the study of Cui et al. [8], they described the parametric illustration to estimate the thermal performance that deals with the counter-flow reformative unintended evaporative heat exchange. It is found that this phenomenon predicts the performance of the counter-flow regenerative IEHX within inconsistency of 12%. Similarly, the impact of hydrogen and production of gasses via ordinary fuels on combustion constraints of a dual fuel diesel

* Corresponding author.
*E-mail addresses:* ideal_riz@hotmail.com, r.haq.qau@gmail.com (R.U. Haq).

http://dx.doi.org/10.1016/j.rinp.2016.11.057
2211-3797/

**Nomenclature**

| | |
|---|---|
| $C$ | specific heat |
| $k$ | thermal conductivity |
| M | Hartmann number |
| R | radius of cylinder |
| Pr | Prandtl number |
| $Re_\omega$ | Reynolds number |
| $I_0$ | Bessel functions of first kind |
| $K_0$ | Bessel functions second kind |
| t | time |
| D | diameter |
| r | radius |
| T | temperature |
| u, v, w | velocity components |
| $\vec{J}$ | current density |
| $\vec{B}$ | magnetic field |
| H | magnetic field intensity |
| L | length of the cylinder |
| P | pressure |
| A | amplitude |
| CNT | carbon nanotube |
| SWCNT | single wall carbon nanotubes |
| MWCNT | multiple wall carbon nanotubes |

*Greek symbols*

| | |
|---|---|
| $\rho$ | density |
| $\mu$ | dynamic viscosity |
| $\nu$ | kinematic viscosity |
| $\sigma$ | electric conductivity |
| $\alpha$ | Womersley Number $(=\sqrt{Re_\omega})$ |
| $\gamma$ | temperature gradient |
| $\phi$ | volume fraction of the nanoparticles |
| $\omega$ | pulsation |

*Subscripts*

| | |
|---|---|
| i | internal |
| e | external |
| f | base fluid |
| p | particle |
| nf | nanofluid |
| f | base fluid |

machine is proposed by Dhole et al. [9]. In fact, the literature reveals vast articles presented by various authors to deal with the heat transfer phenomena; see for example [10–15].

Sanyal and Biswas [16] had proven, under the normal conditions, blood goes with the flow inside the human's cardiovascular structure relies the pumping action of the heart and this system produces a pressure gradient throughout the arteries. Yakhot and Grinberg [17] had examined the effect of pressure gradient rate in the velocity with phase difference along the axial velocity. These phases are differences fluctuate which start from 0 degrees to the small frequencies up to 90° from the highest level of frequencies. Suces et al. [18] numerically examined the reaction features of the temperature at the wall and mean temperature between laminar drift and a horizontal plate by mean of finite difference method (FDM). Latham [19] was the first researcher who discussed the peristaltic flow. Later on, several researchers and scientists emphasized their considerations to analysis the peristaltic flows with different fluid models and geometries. Majdalani [20] resolved the precise solution of limiting case of Navier-Stokes equation that governs the pulsatile glide through a pipe; and stress gradient is changed by using the Fourier coefficients. Agrawal and Anwaruddin [21] present a mathematical model that deals with the impact of magnetic strength of the blood flow via similarly branched channel with different partitions. They have observed that magnetic strength also used in a blood pumping of wearing out cardiac processes to treatment few diseases of arteries. Tzirtzilakis [22] discussed the mathematical model for bio-magnetic fluid, appropriate for description of Newtonian blood float beneath the motion of magnetic field. Ramamurthy and Shanker [23] studied the magneto-hydrodynamic (MHD) results in blood flow via a porous channel.

In the recent development of science and technology, study of nanofluid attained considerable attention due to its wide applications. Nanofluid is just a fluid comprising nanometer-sized particles, referred to as nanoparticles. One of the most important features of nanofluid is to enhance the heat transfer by improving the thermal conductivity of working fluids. This invention was first conceived by Choi [24]. Nanofluids require some important thermos-physical properties of both particle and fluid such as: thermal diffusivity, viscosity, thermal conductivity, and convective heat transfer coefficients comparable; for more details see [25–28]. Buongiorno [29] presented after effect of heat alteration on the carriage of nanofluid via important slip mechanism. Akbar et al. [30] discussed the mixed convection flow of Jeffrey nanofluid with magnetic field effects. Emad and Ebaid [31] discussed about nanofluids within the boundary layer region and exact solution acquired from the governing equation with distinct values of emerging physical parameters. Recently, various authors have developed theoretical and experimental study regarding nanofluids according to necessity of industrial demand [32–40].

The CNTs are one of the most important and significant material in the form of tubular cylinder of carbon atoms having astonishing mechanical, electrical and thermal performance. The CNTs can appearance high achievement because of their amazing electronic, mechanical, and structural backdrop such as baby admeasurement and mass, stronger, higher electrical and thermal conductivity, and so forth [41]. The carbon atoms that anatomy nanotubes are abiding in a hexagonal network 1 nm in bore and 100 m in length can about be anticipation of as a band of graphite formed up into a cylinder [42]. There are three types of CNTs: single, double and multiple wall carbon nanotubes, which alter in the adjustment of their graphene cylinders. According to latest research of Elena et al. [43], only saturation of nanoparticles is not enough to enhance the heat transfer. They have discussed the thermal conductivity of various shapes of particle. They conclude that plats shape particle provides best and higher thermal conductivity as compared to the other of shapes of the particles. In agreement with Murshed et al. [44], it is found that CNTs have approximately six times superior thermal conductivity as compared to the other base fluids and materials at room temperature. Mainly, the benefits of CNT include additives in polymers, lithium-battery anodes, nanolithography, super capacitor, hydrogen storage, electromagnetic-wave absorption and shielding gas-discharge tubes in telecom networks. Apart from these CNTs can be used for quantum dots, drug delivery, drug discovery, implantable Nano sensors and Nano robots, actuators and Nano fluidic system.

In view of above literature survey, the main objective of the present framework is to analyze the heat transfer of engine oil based CNTs between two concentric cylinders. Two kinds of nanoparticles namely SWCNTs and MWCNTs are analyzed within the base

fluid. Flow is generated due to oscillatory pressure gradient. The governing equations of the described model are then solved analytically to achieve the precise answers of Bessel function of first and second kind. The obtained expressions for velocity, temperature and pressure gradient are discussed graphically through variant in bodily parameters. Dominant difference can be found in the velocity and temperature profiles for each mixture: engine oil-SWCNTs and engine oil-MWCNTs. Pressure gradient is also calculated for different values of time.

## Mathematical formulation

### *Physical problem*

An electrically conducting viscous, incompressible fluid is flowing between two concentric cylinders is shown in Fig. 1. Fluid is moving within the concentric cylinder due to pulsatile pressure gradient and constant magnetic field that is applied in the direction of $z$-axis. In the beginning, the inner cylinder is at a temperature of 400 K and the outer cylinder has adiabatic condition with atmospheric pressure and a temperature of 300 K.

### *Governing equations*

We have considered incompressible, viscous and electrically conducting fluid, and the flow is laminar and symmetric in both directions. By neglecting the energy losses because of law of conservation of mass, and the constant magnetic field is acting in the radial direction. The conventional continuity, momentum and energy equations are, respectively, given by

$$\nabla\cdot\vec{V}=0, \tag{1}$$

$$\rho_{nf}\left(\frac{\partial\vec{V}}{\partial t}+\vec{V}\cdot\nabla\vec{V}\right)=-\nabla P+\mu_{nf}\nabla^2\vec{V}+(\vec{J}\times\vec{B})\vec{V}, \tag{2}$$

$$(\rho C)_{nf}\left(\frac{\partial T_f}{\partial t}+\vec{V}\cdot\nabla T\right)=k_{nf}\nabla^2 T. \tag{3}$$

In cylindrical coordinates system, equation of continuity, momentum and energy are given to be:

$$\frac{\partial u}{\partial r}+\frac{\partial w}{\partial z}+\frac{u}{r}=0, \tag{4}$$

$$\rho_{nf}\left(\frac{\partial u}{\partial t}+u\frac{\partial u}{\partial r}+w\frac{\partial u}{\partial z}\right)=-\frac{\partial P}{\partial r}+\mu_{nf}\left(\frac{\partial^2 u}{\partial r^2}+\frac{1}{r}\frac{\partial u}{\partial r}+\frac{\partial^2 u}{\partial z^2}-\frac{u}{r^2}\right), \tag{5}$$

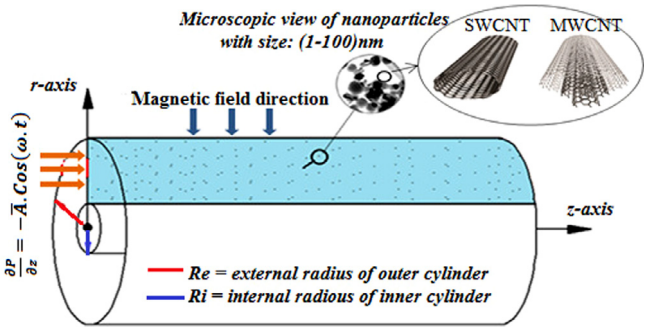


**Fig. 1.** Geometry of the problem.

$$\rho_{nf}\left(\frac{\partial w}{\partial t}+u\frac{\partial w}{\partial r}+w\frac{\partial w}{\partial z}\right)=-\frac{\partial P}{\partial z}+\mu_{nf}\left(\frac{\partial^2 w}{\partial r^2}+\frac{1}{r}\frac{\partial w}{\partial r}+\frac{\partial^2 w}{\partial z^2}\right)-\sigma_{nf}B_o^2 w, \tag{6}$$

$$(\rho C)_{nf}\left(\frac{\partial T}{\partial t}+u\frac{\partial T}{\partial r}+w\frac{\partial T}{\partial z}\right)=k_{nf}\left(\frac{\partial^2 T}{\partial r^2}+\frac{1}{r}\frac{\partial T}{\partial r}+\frac{\partial^2 T}{\partial z^2}\right). \tag{7}$$

In the above equations $u$ and $w$ are velocities along $r$ and $z$ direction, respectively, $P$ and $T$ are the pressure and temperature. Here, $\rho_{nf},\mu_{nf},(\rho C)_{nf},k_{nf}$ and $\sigma_{nf}$ are density, viscosity, specific heat, thermal and electric conductivity of nanofluid, respectively. Moreover, we have

$$\rho_{nf}=(1-\phi)\rho_f+\phi\rho_{CNT}, \tag{8a}$$

$$(\rho C)_{nf}=(1-\phi)(\rho C)_f+\phi(\rho C)_{CNT}, \tag{8b}$$

$$\frac{k_{nf}}{k_f}=\frac{1-\phi+2\phi\left(\frac{k_{CNT}}{k_{CNT}-k_f}\right)ln\left(\frac{k_{CNT}+k_f}{2k_f}\right)}{1-\phi+2\phi\left(\frac{k_f}{k_{CNT}-k_f}\right)ln\left(\frac{k_{CNT}+k_f}{2k_f}\right)}, \tag{8c}$$

$$\mu_{nf}=\frac{\mu_f}{(1-\phi)^{2.5}}. \tag{8d}$$

In the above expressions $\rho_f,C_f,k_f,\mu_f$ are the density, specific heat, thermal conductivity, dynamic viscosity of working fluid, respectively. Similarly, $\rho_{CNT},C_{CNT},k_{CNT}$ are the density, specific heat, thermal conductivity of the fluid, thermal conductivity of the CNT, respectively. Notice that $\phi$ is nanoparticle volume fraction. In view of above mentioned quantities, the conservation law of momentum and energy are reduced to

$$\left((1-\phi)\rho_f+\phi\rho_{CNT}\right)\left(\frac{\partial u}{\partial t}+u\frac{\partial u}{\partial r}+w\frac{\partial u}{\partial z}\right)=-\frac{\partial P}{\partial r}+\frac{\mu_f}{(1-\phi)^{2.5}}\left(\frac{\partial^2 u}{\partial r^2}+\frac{1}{r}\frac{\partial u}{\partial r}+\frac{\partial^2 u}{\partial z^2}-\frac{u}{r^2}\right), \tag{9a}$$

$$\left((1-\phi)\rho_f+\phi\rho_{CNT}\right)\left(\frac{\partial w}{\partial t}+u\frac{\partial w}{\partial r}+w\frac{\partial w}{\partial z}\right)=-\frac{\partial P}{\partial z}+\frac{\mu_f}{(1-\phi)^{2.5}}\left(\frac{\partial^2 w}{\partial r^2}+\frac{1}{r}\frac{\partial w}{\partial r}+\frac{\partial^2 w}{\partial z^2}\right)-\sigma_f B_o^2 w, \tag{9b}$$

$$\left((1-\phi)(\rho C)_f+\phi(\rho C)_{CNT}\right)\left(\frac{\partial T}{\partial t}+u\frac{\partial T}{\partial r}+w\frac{\partial T}{\partial z}\right)=k_{nf}\left(\frac{\partial^2 T}{\partial r^2}+\frac{1}{r}\frac{\partial T}{\partial r}+\frac{\partial^2 T}{\partial z^2}\right). \tag{9c}$$

Notice that the system can be expressed in dimensionless terms by defining the following quantities:

$$u=\frac{u'}{\omega R_e},\ w=\frac{w'}{\omega R_e},\ r=\frac{r'}{R_e},\ z=\frac{z'}{R_e},\ t=\omega t',\ T=\frac{T'-T_f}{T_i-T_f},$$
$$P=\frac{P'}{\rho_f R_e^2\omega^2},\ \nu_f=\frac{\mu_f}{\rho_f},\ Pr=\frac{\mu_f C_f}{k_f},\ M=R_e B_o\sqrt{\frac{\sigma_f}{\mu_f}},\ Re_\omega=\alpha^2=\frac{\omega R_e^2}{\nu_f}.$$

In the above expression $Re_\omega$ is the Reynolds number, $Pr$ is the Prandtl number and $M$ is the Hartmann number. Dimensionless form of the Eqs. 9(a)–9(c) should take the following forms:

$$A_1\left(\frac{\partial u}{\partial t}+u\frac{\partial u}{\partial r}+w\frac{\partial u}{\partial z}\right)=-\frac{\partial P}{\partial r}+\frac{1}{(1-\phi)^{2.5}Re_\omega}\left(\frac{\partial^2 u}{\partial r^2}+\frac{1}{r}\frac{\partial u}{\partial r}+\frac{\partial^2 u}{\partial z^2}-\frac{u}{r^2}\right), \tag{10a}$$

$$A_1\left(\frac{\partial w}{\partial t}+u\frac{\partial w}{\partial r}+w\frac{\partial w}{\partial z}\right)=-\frac{\partial P}{\partial z}+\frac{1}{(1-\phi)^{2.5}Re_\omega}\left(\frac{\partial^2 w}{\partial r^2}+\frac{1}{r}\frac{\partial w}{\partial r}+\frac{\partial^2 w}{\partial z^2}\right)-\frac{M^2 w}{Re_\omega}, \tag{10b}$$

$$A_2\left(\frac{\partial T}{\partial t}+u\frac{\partial T}{\partial r}+w\frac{\partial T}{\partial z}\right)=\frac{A_3}{PrRe_\omega}\left(\frac{\partial^2 T}{\partial r^2}+\frac{1}{r}\frac{\partial T}{\partial r}+\frac{\partial^2 T}{\partial z^2}\right). \tag{10c}$$

where, the coefficients $A_1, A_2$ and $A_3$ are defined as:

$$A_1=(1-\phi)+\phi\frac{\rho_{CNT}}{\rho_f}, \tag{11a}$$

$$A_2=(1-\phi)+\phi\frac{(\rho C)_{CNT}}{(\rho C)_f}, \tag{11b}$$

$$A_3=\frac{k_{nf}}{k_f}=\frac{1-\phi+2\phi\left(\frac{k_{CNT}}{k_{CNT}-k_f}\right)ln\left(\frac{k_{CNT}+k_f}{2k_f}\right)}{1-\phi+2\phi\left(\frac{k_f}{k_{CNT}-k_f}\right)ln\left(\frac{k_{CNT}+k_f}{2k_f}\right)}. \tag{11c}$$

*Boundary conditions*

The associated initial and boundary conditions to the model will take the following form:

At $t=0$

$$u(r,z,0)=w(r,z,0)=0 \text{ and } p(r,z,0)=T_f(r,z,0)=0, \tag{12a}$$

For external duct:

$$u(1,z,t)=w(1,z,t)=0 \text{ and } \frac{\partial T_f}{\partial r}(1,z,t)=0. \tag{12b}$$

For internal duct:

$$u\left(\frac{R_i}{R_e},z,t\right)=w\left(\frac{R_i}{R_e},z,t\right)=0, \text{ and } T_f\left(\frac{R_i}{R_e},z,t\right)=1. \tag{12c}$$

To find the analytical solution of the present model, we have assumed that flow is fully developed and velocity field is defined as:

$$\vec{V}=[0,0,w(r,z,t)]. \tag{13}$$

The simplified form of governing equations can be rewrite in the following form,

$$A_1\frac{\partial w}{\partial t}=-\frac{\partial p}{\partial z}-\frac{1}{(1-\phi)^{2.5}Re_\omega}\left(\frac{\partial^2 w}{\partial r^2}+\frac{1}{r}\frac{\partial w}{\partial r}\right)-\frac{M^2}{Re_\omega}w, \tag{14a}$$

$$A_2\left(\frac{\partial T}{\partial t}+w\frac{\partial T}{\partial z}\right)=\frac{A_3}{PrRe}\left(\frac{\partial^2 T}{\partial r^2}+\frac{1}{r}\frac{\partial T}{\partial r}+\frac{\partial^2 T}{\partial z^2}\right). \tag{14b}$$

As flow problem is axis-symmetry, this analysis could be reduced within the annular space between two concentric cylinders. The dimensionless form of Eqs. (14a) and (14b) becomes:

$$A_1\frac{\partial w}{\partial t}=-\frac{\partial p}{\partial z}-\frac{A_4}{\alpha^2}\left(\frac{\partial^2 w}{\partial r^2}+\frac{1}{r}\frac{\partial w}{\partial r}\right)-\frac{M^2}{\alpha^2}w, \tag{15a}$$

$$A_2\left(\frac{\partial T}{\partial t}+w\frac{\partial T}{\partial z}\right)=\frac{A_3}{Pr\alpha^2}\left(\frac{\partial^2 T}{\partial r^2}+\frac{1}{r}\frac{\partial T}{\partial r}+\frac{\partial^2 T}{\partial z^2}\right), \tag{15b}$$

where $A_4=\frac{1}{(1-\phi)^{2.5}}$.

*Solution of the problem*

Since the present phenomena deals with the study of pulsatile flow, the pressure gradient might be expressed in the form:

$$\frac{\partial \mathbf{P}}{\partial \mathbf{z}}=-\bar{A}\cdot Cos(\omega\cdot t)=Real(-\bar{A}e^{i\omega t}). \tag{16}$$

The supposed form solution for velocity profile can be defined as

$$w(r,t)=Real(f(r)e^{i\omega t}). \tag{17}$$

In view of the above equations, we may conclude from Eq. (15a)

$$\frac{d^2 f(r)}{dr^2}+\frac{1}{r}\frac{df(r)}{dr}-\frac{1}{A_4}(M^2+i\alpha^2 A_1)f(r)=-\frac{1}{A_4}\bar{A}\alpha^2. \tag{18}$$

It is clearly seen that the solution obtained from Eq. (18) is in the shape of Bessel function, that is:

$$f(r)=C_1 I_0(\zeta r)+C_2 K_0(\zeta r), \tag{19}$$

where $I_0$ Bessel functions of first kind and $K_0$ are Bessel functions second kind and $\zeta=\sqrt{M^2+i\alpha^2 A_1}$. To determine $C_1$ and $C_2$, we use the boundary conditions

$$r=\frac{R_i}{R_e}=R_i^* r=1 \quad w=0. \tag{20}$$

From Eq. (17) velocity solution profile can be indicted as

$$w(r,t)=Real\left[C_1 I_0(\zeta r)+C_2 K_0(\zeta r)+\frac{\bar{A}\alpha^2}{A_4\zeta^2}\right]e^{it}, \tag{21}$$

where

$$C_1=-\frac{\alpha^2 BesselK[0,\zeta]\bar{A}-\alpha^2 BesselK[0,\zeta R^*]\bar{A}}{\zeta^2(BesselI[0,\zeta R^*]BesselK[0,\zeta]-BesselI[0,\zeta]BesselK[0,\zeta R^*])A_4},$$

$$C_2=-\frac{-\alpha^2 BesselI[0,\zeta]\bar{A}+\alpha^2 BesselI[0,\zeta R^*]\bar{A}}{\zeta^2(BesselI[0,\zeta R^*]BesselK[0,\zeta]-BesselI[0,\zeta]BesselK[0,\zeta R^*])A_4}.$$

To determine the analytical solution of Eq. (15b), we assume that solution of temperature profile can be represented as:

$$T(r,z,t)=Real\left[-\gamma^* z+\gamma^* g(r)e^{it}+1\right], \tag{22}$$

where $\gamma^*=\frac{Re}{L}$. Using Eq. (15b) we have

$$\frac{d^2 g(r)}{dr^2}+\frac{1}{r}\frac{dg(r)}{dr}-i\frac{A_2\alpha^2 Pr}{A_3}g(r)=\frac{A_2\alpha^2 Pr}{A_3}f(r). \tag{23}$$

Using the boundary conditions,

$$r=R_i^*\Rightarrow T=1 \text{ and } r=1\Rightarrow\frac{\partial T}{\partial r}=0, \tag{24}$$

we have assumed that the solution of temperature profile can be indicated as:

$$\left.\begin{aligned}T(r,z,t)=Real[&-\gamma^* z+\gamma^*[-iC_1 I_0(\zeta r)-iC_2 K_0(\zeta r)+C_3 I_0(\xi r)\\&+C_4 K_0(\xi r)-\tfrac{i\bar{A}\alpha^2}{\zeta^2}]e^{it}+1]\end{aligned}\right\} \tag{25}$$

where

$$\xi=\alpha\sqrt{\frac{iPrA_2}{A_3}},$$

$$C_3 = \frac{\alpha\zeta^2\sqrt{\mathrm{iPr}}\sqrt{A_2}A_4\mathrm{BesselK}[1,\xi]\delta_1 + \zeta^3\sqrt{A_3}A_4\mathrm{BesselK}[0,\xi R^*]\delta_2}{\alpha\zeta^2\sqrt{\mathrm{iPr}}(\mathrm{BesselI}[1,\xi]\mathrm{BesselK}[0,\xi R^*] + \mathrm{BesselI}[0,\xi R^*]\mathrm{BesselK}[1,\xi])},$$

$$C_4 = \frac{\alpha\zeta^2\sqrt{\mathrm{iPr}}\sqrt{A_2}A_4\mathrm{BesselI}[1,\xi]\delta_1 - \delta_2 = i[\mathrm{BesselI}[1,\zeta]C_1 - \mathrm{BesselK}[1,\zeta]C_2].\zeta\sqrt{A_3}A_4\mathrm{BesselI}[0,\xi R^*]\delta_2}{\alpha\zeta^2\sqrt{\mathrm{iPr}}(\mathrm{BesselI}[1,\xi]\mathrm{BesselK}[0,\xi R^*] + \mathrm{BesselI}[0,\xi R^*]\mathrm{BesselK}[1,\xi])},$$

$$\delta_1 = i\left[\mathrm{BesselI}[0,\zeta R^*]C_1 + \mathrm{BesselK}[0,\zeta R^*]C_2 + \frac{\alpha^2}{A_4\zeta^2}\bar{A} - \mathrm{i}\frac{z}{e^{\mathrm{it}}}\right],$$

$$\delta_2 = i[\mathrm{BesselI}[1,\zeta]C_1 - \mathrm{BesselK}[1,\zeta]C_2]$$

*Pressure calculation*

From Eq. (15a) we have

$$\frac{\partial P}{\partial z} = -\bar{A}_1\frac{\partial w}{\partial t} + \frac{A_4}{\alpha^2}\left[\frac{\partial^2 w}{\partial r^2} + \frac{1}{r}\frac{\partial w}{\partial r}\right] - \frac{M^2 w}{\alpha^2}. \tag{26}$$

**Table 1**
Thermo physical properties of different base fluids and CNTs.

| Phase | $\rho$ (kg/m$^3$) | K (W/mK) | C (J/kg K) |
|---|---|---|---|
| Engine oil (Base fluid) | 884 | 0.144 | 1910 |
| SWCNT(Nanoparticles) | 2600 | 6600 | 425 |
| MWCNT(Nanoparticles) | 1600 | 3000 | 796 |

Substituting the solution obtained for $w(r,t)$ in Eq. (26)

$$\begin{aligned}\frac{\partial P}{\partial z} = &-A_1\left(\mathrm{ie}^{\mathrm{it}}\left(\frac{\mathrm{BesselI}[0,r\zeta]c_1}{\zeta^2A_4^2} - \frac{\mathrm{BesselK}[0,r\zeta]c_2}{\zeta^2A_4^2} + \frac{\alpha^2 * \bar{A}}{(A_4^2 * \zeta^2)}\right)\right)\\ &+\frac{A_4}{\alpha^2}\left(\mathrm{e}^{\mathrm{it}}\left(\frac{(\mathrm{BesselI}[0,r\zeta] + \mathrm{BesselI}[2,r\zeta])c_1}{2A_4^2}\right.\right.\\ &\left.+\frac{(-\mathrm{BesselK}[0,r\zeta] - \mathrm{BesselK}[2,r\zeta])c_2}{2A_4^2}\right)\\ &+\frac{1}{r}\mathrm{e}^{\mathrm{it}}\left(\frac{\mathrm{BesselI}[1,r\zeta]c_1}{\zeta A_4^2} + \frac{\mathrm{BesselK}[1,r\zeta]c_2}{\zeta A_4^2}\right)\Bigg)\\ &-\frac{M^2}{\alpha^2}\mathrm{e}^{\mathrm{it}}\left(\mathrm{BesselI}[0,r\times\zeta]\frac{1}{(A_4^2\zeta^2)}C_1 - \mathrm{BesselK}[0,r\times\zeta]\frac{1}{(A_4^2\zeta^2)}c_2 + \frac{\alpha^2\bar{A}}{(A_5^2\eta^2)}\right)\end{aligned} \tag{27}$$

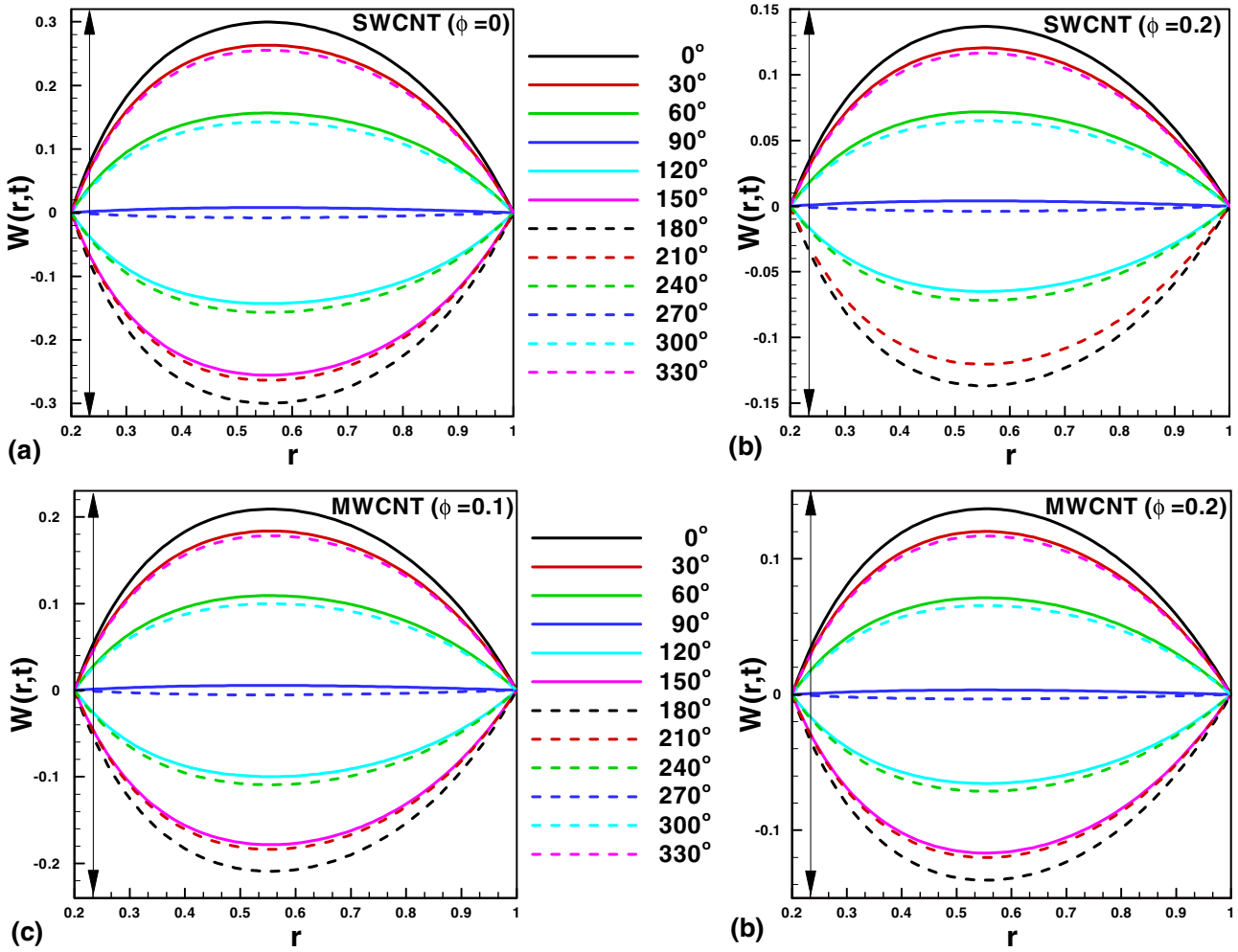


**Fig. 2.** Variation of velocity profile when $M = 5, Re_\omega = 1$: (a) SWCNT ($\phi = 0$), (b) SWCNT ($\phi = 0.2$), (c) MWCNT ($\phi = 0.1$) (d) MWCNT ($\phi = 0.2$).

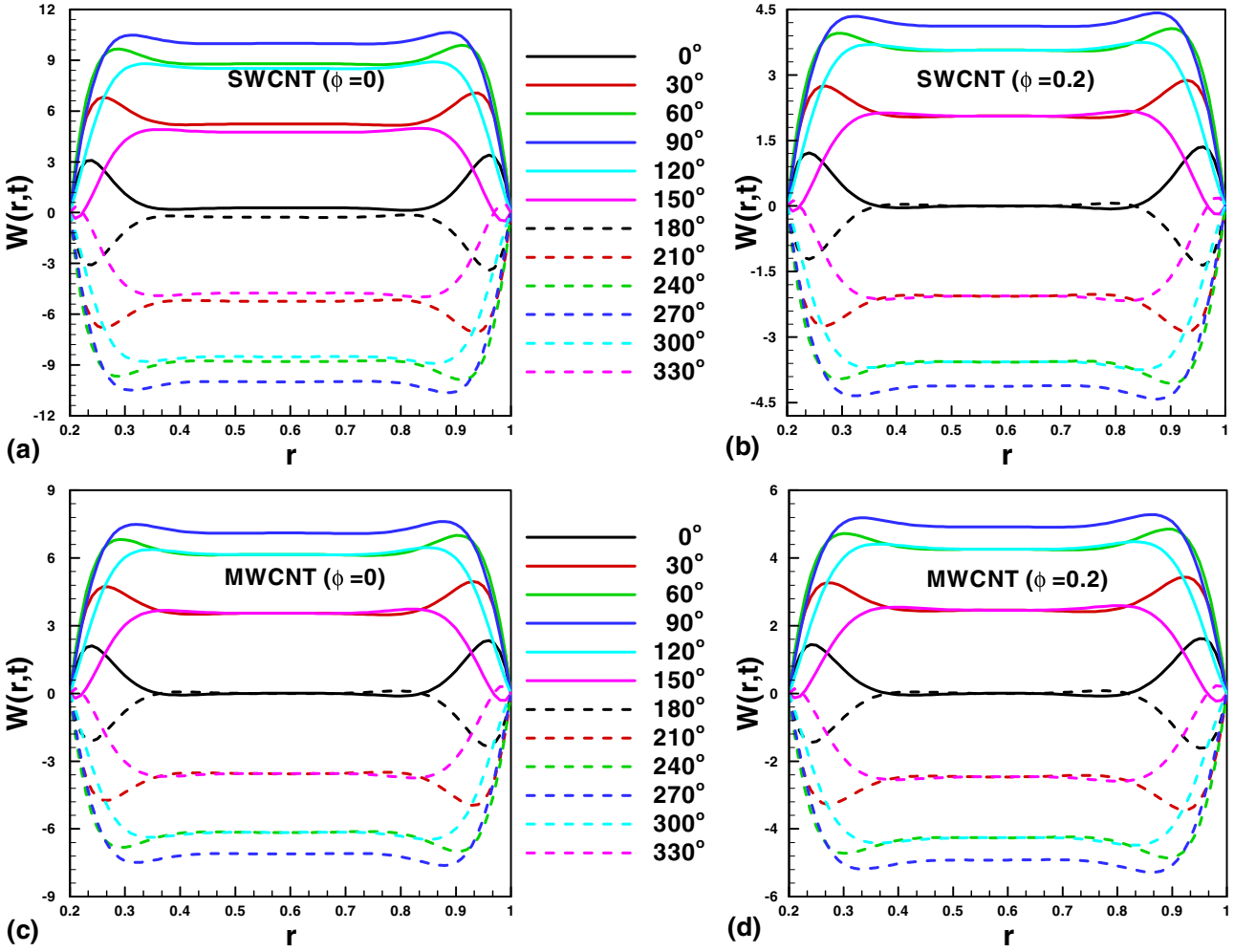


**Fig. 3.** Variation of velocity profile when $M = 5, Re_{\omega} = 30$ (a) SWCNT ($\phi = 0$), (b) SWCNT ($\phi = 0.2$), (c) MWCNT ($\phi = 0$), (d) MWCNT ($\phi = 0.2$).

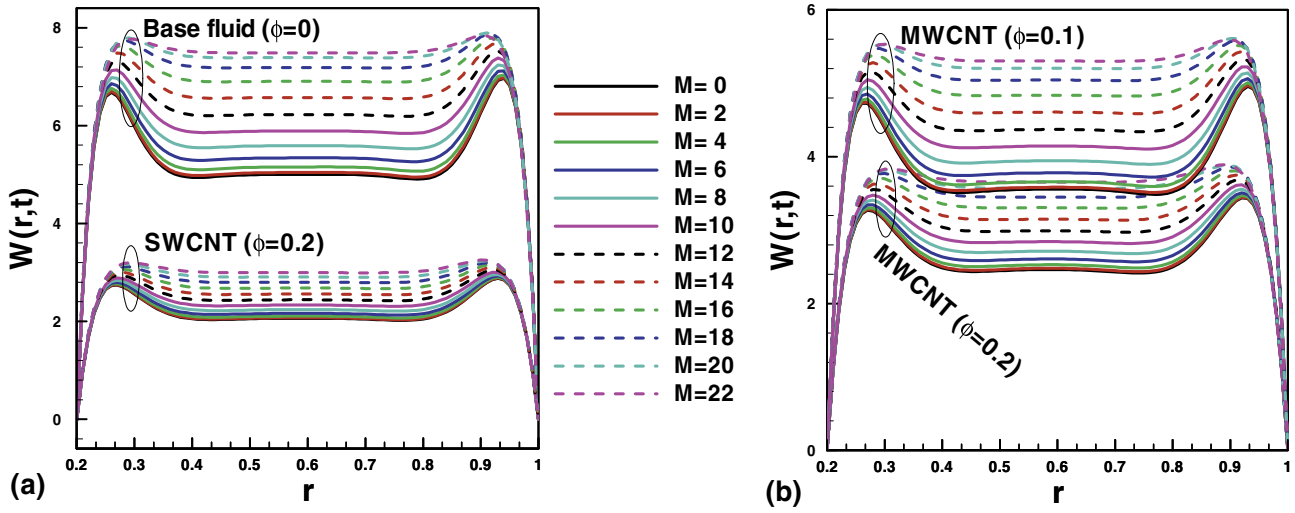


**Fig. 4.** Variation of velocity profile for various values of $M$ when $t = 30^{\circ}, Re_w = 30$ (a) SWCNT (b) MWCNT.

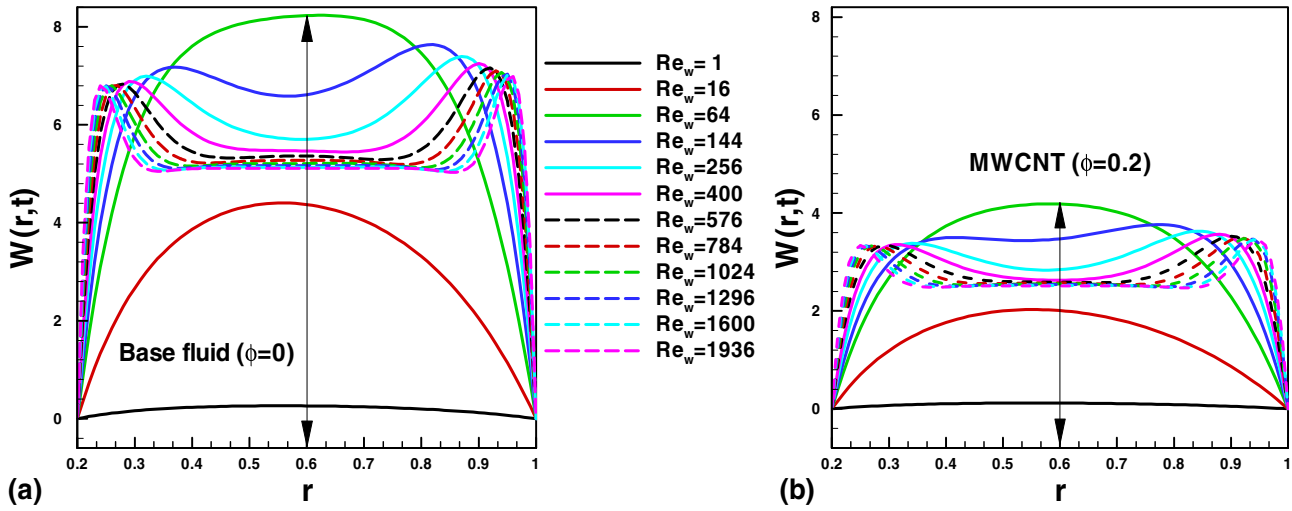


**Fig. 5.** Variation of velocity profile for various values of $Re_w$ when $t = 30°, M = 30$ (a) Base fluid ($\phi = 0$), and (b) MWCNT ($\phi = 0.2$).

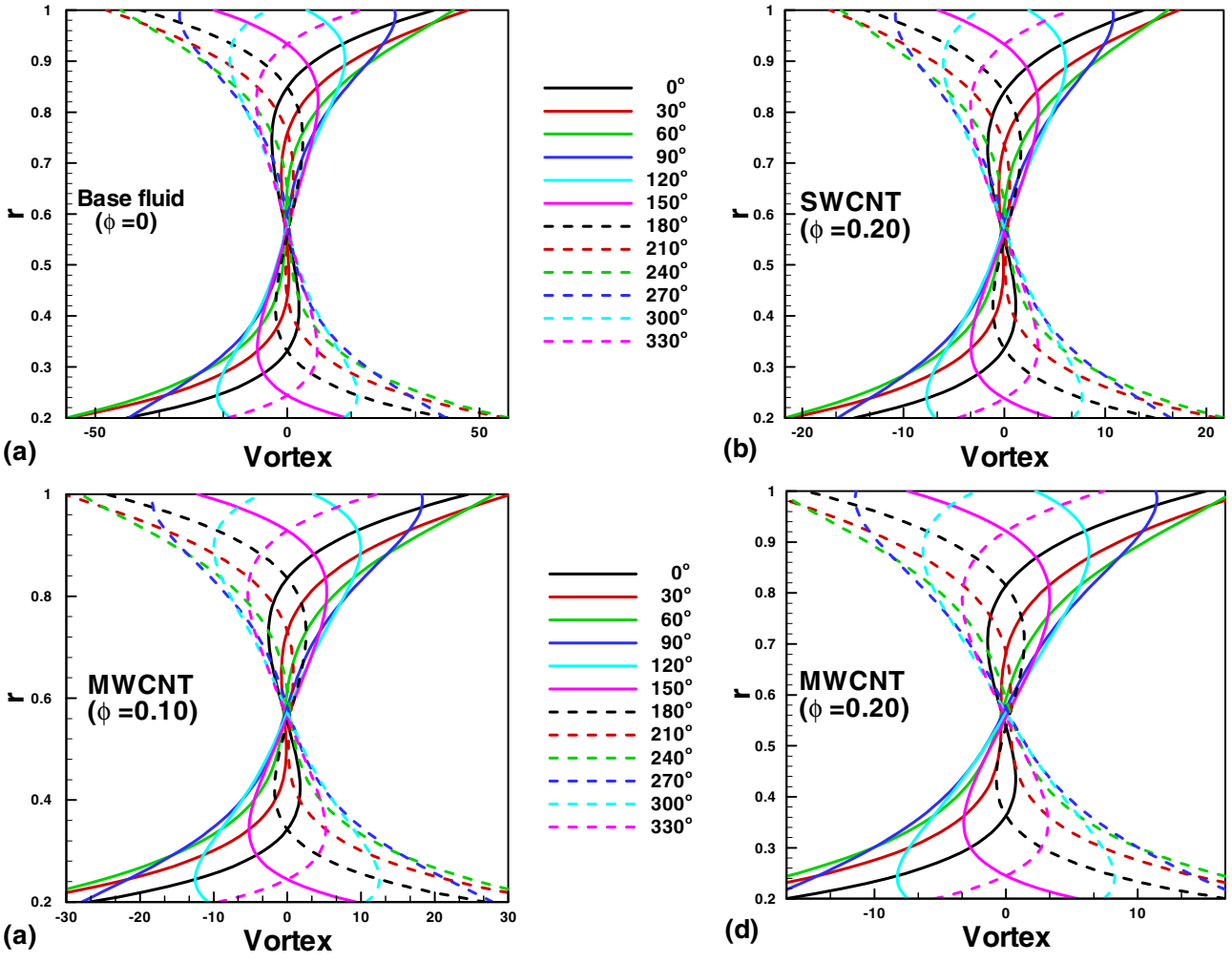


**Fig. 6.** Variation of vortex profile $t$ for (a) Pure fluid ($\phi = 0$), (b) SWCNT ($\phi = 0.2$), (c) MWCNT ($\phi = 0.1$), (d) MWCNT ($\phi = 0.2$) when $Re_\omega = 10, M = 5$.

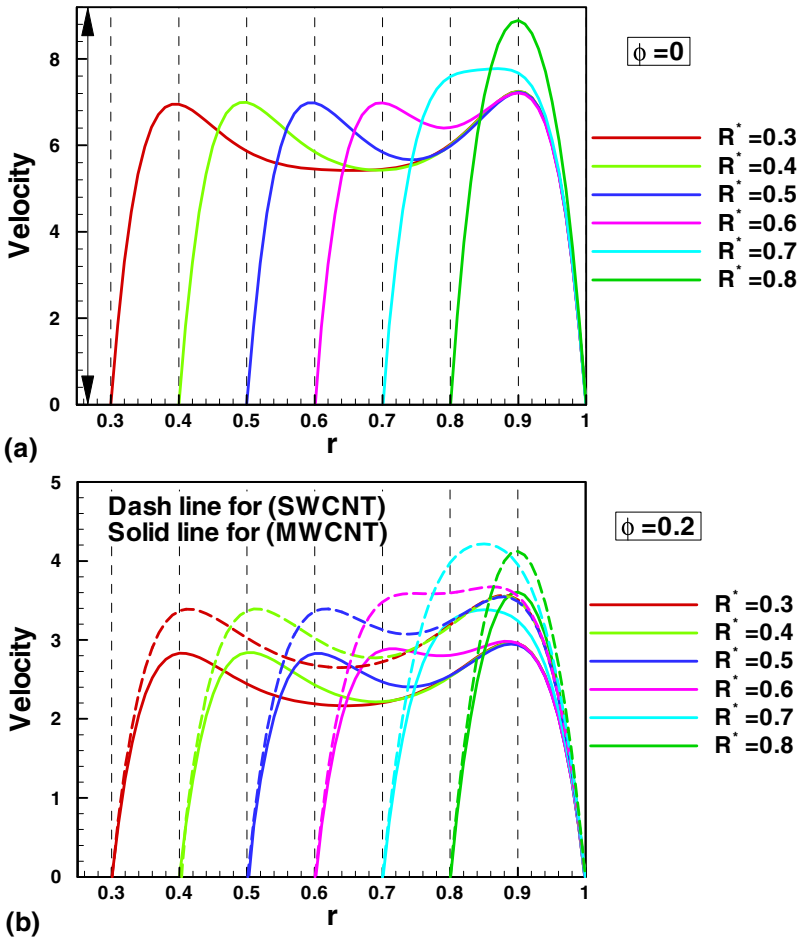


**Fig. 7.** Variation of velocity profile for various values of $R^*$ (a) Pure fluid ($\phi = 0$) (b) SWCNT and MWCNT ($\phi = 0.2$).

The dimensionless pressure rise is defined as

$$\Delta P = \int_0^1 \frac{\partial p}{\partial z} dz, \tag{28}$$

$$\begin{aligned} P = {} & -A_1 i e^{it}\left(\frac{\alpha^2 \bar{A}}{\zeta^2 A_4^2} + \frac{\text{BesselI}[0, r\zeta]c_1}{\zeta^2 A4_4^2} - \frac{\text{BesselK}[0, r\zeta]C_2}{\zeta^2 A_4^2}\right) \\ & + \frac{A_4}{\alpha^2}\left(e^{it}\left(\frac{(\text{BesselI}[0, r\zeta] + \text{BesselI}[2, r\zeta])C_1}{2A_4^2}\right.\right. \\ & \left. + \frac{(-\text{BesselK}[0, r\zeta] - \text{BesselK}[2, r\zeta])C_2}{2A_4^2}\right) \\ & \left. + \frac{1}{r} e^{it}\left(\frac{\text{BesselI}[1, r\zeta]C_1}{\zeta A_4^2} + \frac{\text{BesselK}[1, r\zeta]C_2}{\zeta A_4^2}\right)\right) \\ & - \frac{M^2}{\alpha^2} e^{it}\left(\text{BesselI}[0, r \times \zeta]\frac{C_1}{(A_4^2\zeta^2)} - \text{BesselK}[0, r \times \zeta]\frac{C_2}{(A_4^2\zeta^2)} + \frac{\alpha^2 \bar{A}}{(A_4^2\zeta^2)}\right) \end{aligned} \tag{29}$$

Expression for stream function is given as follows:

$$w(r, t) = \frac{1}{r}\frac{\partial \psi}{\partial r}. \tag{30}$$

## Results and discussion

In order to obtain an insight into the physics of the problem, numerical computations are conducted for velocity profile, temperature profile, vorticity, pressure rise, stream lines, skin-friction and Nusselt number are plotted for varied values of magnetic field parameter $M$, kinetic Reynolds number $Re_\omega$, nanoparticle volume fraction $\phi$, amplitude of pressure gradient $\bar{A}$ and Prandtl number Pr. To obtain the required velocity and temperature profiles, thermos-physical values of CNTS and based fluids are presented in Table 1.

We studied the axial velocities which vary from inlet to outlet and affect the heat transfer rate region due to development of flow. For one complete pulsation cycle of 360° the instances were taken at each $t = 30$ to calculate the axial velocity variation at particular volume fraction $\phi$. All the captured instances are in total 12 for a complete cycle of 360°. Fig. 2(a)–(d) are ready to study the impact of various values of nanofluid volume fraction on velocity profile. Each figure depicts the velocity profile traced a parabolic trajectory with maximum values at the mean position of the channel and rapidly decreases with rise of $\phi$. It is illustrated from Fig. 2(a)–(d) that inclusion of nanoparticles provides the increase of density of whole mixture. In Fig. 2(a), one can observe through margin line that there is a significant and higher disturbance in the velocity profile for base fluid ($\phi = 0$) as compared to the nonzero values of nanoparticle volume fraction. Physically, we can say that by incorporating the nanoparticles (both SWCNTs and MWCNTs) within the engine-oil then the density of whole mixture will increase considerably. Consequently, when density of nanofluid increases then motion of nanofluid becomes slow as compared to the base fluid (engine-oil), as shown in Fig. 2(a)–(c).

Figs. 3(a)–(d) depicts the distribution of velocity for both SWCNTs and MWCNTs when $\phi = 0$ and $\phi = 0.2$. If we compare Fig. 2 with Fig. 3 then velocity profile becomes high with the

increase of Womersley number, $\sqrt{Re_\omega}$. It is also referred to from Fig. 3 that incorporation of nanoparticles diminishes the velocity of the Engine oil $\phi = 0$. It is shown that with increase of $Re_w$ velocity slightly deviate from sinusoidal mean velocity for certain instances of time. Additionally, the increase of $Re_w$ gives rise to more substantial annular effect so that the radial velocity nearby cylinder wall become steeper and friction force increases with the increase of $Re_w$. Inertial component increases in momentum equation with the increase of $Re_\omega$. Further, it is noticed that by the increase of Womersley number, velocity profile shows the increasing behavior. Since, Womersley number is the ratio of pulsation to the viscous forces, increasing the Womersley number reduces the viscous forces. Hence, when viscous forces reduce then motion of the fluid particles become faster and consequently velocity profile will increase gradually; see Fig. 3(a)–(d).

Fig. 4(a)–(d) show the velocity distribution for Hartmann number $M$ while rest of the parameters are kept fixed. Per the physical phenomena, increasing the strength of magneto-hydrodynamic $M$ leads to increase the velocity of nanofluid near the mean position of the channel. However, near the lower and upper surfaces of the channel, velocity of nanofluid certainly rise and met the surface of channel at zero. It can be identified from Fig. 4(a)–(d) that adjunct of nanoparticles decreases the velocity engine oil. Further it is observed from Fig. 4(a), that engine oil-SWCNT ($\phi = 0.2$) have comparatively low velocity as compared to the engine oil ($\phi = 0$). Similar behavior can be observed in Fig. 4(b). Fig. 5(a)–(b), demonstrate the variation of Womersley number $\alpha = \sqrt{Re_w}$ to analyze the flow velocity for both base fluid and nanofluid. Fig. 5(a) shows that increasing Womersley number leads to increasing behavior near the surface of the duct. On the other hand, at the mean position, the behavior of velocity profile rapidly increase for small values of Womersley number while it is stable for large values of Womersley number. In comparison to Fig. 5(a), it is found in Fig. 5(b) that the behavior of velocity profile remains the same for engine oil-MWCNT ($\phi = 0.2$) but velocity remains low.

The variation of vortex profiles attained in the current study has similar results to that presented by Majdalani [11]. Though, existence of minor variation is virtue of fact that Majdalani [11] desig $\phi = 0.2$ n through pulsatile drift passed in a rectangular duct. Fig. 6 (a)–(d) indicates the influence of volume fraction $\phi$ on the radial profile of vorticity. We note that the magnitude of the vortices is higher when the volume fraction $\phi$ for nanofluid is small. It should be noted that the vorticity takes negative values for certain phases for different values of $\phi$ indicating the presence of a return flow. In comparison to Fig. 6(a)–(d), the obtained variation in vortex is very high for base fluid ($\phi = 0$) as compared to the non-zero values of nanoparticle volume fraction. Similarly, engine-oil based SWCNT ($\phi = 0.2$) have higher disturbance in the vortex as compared to

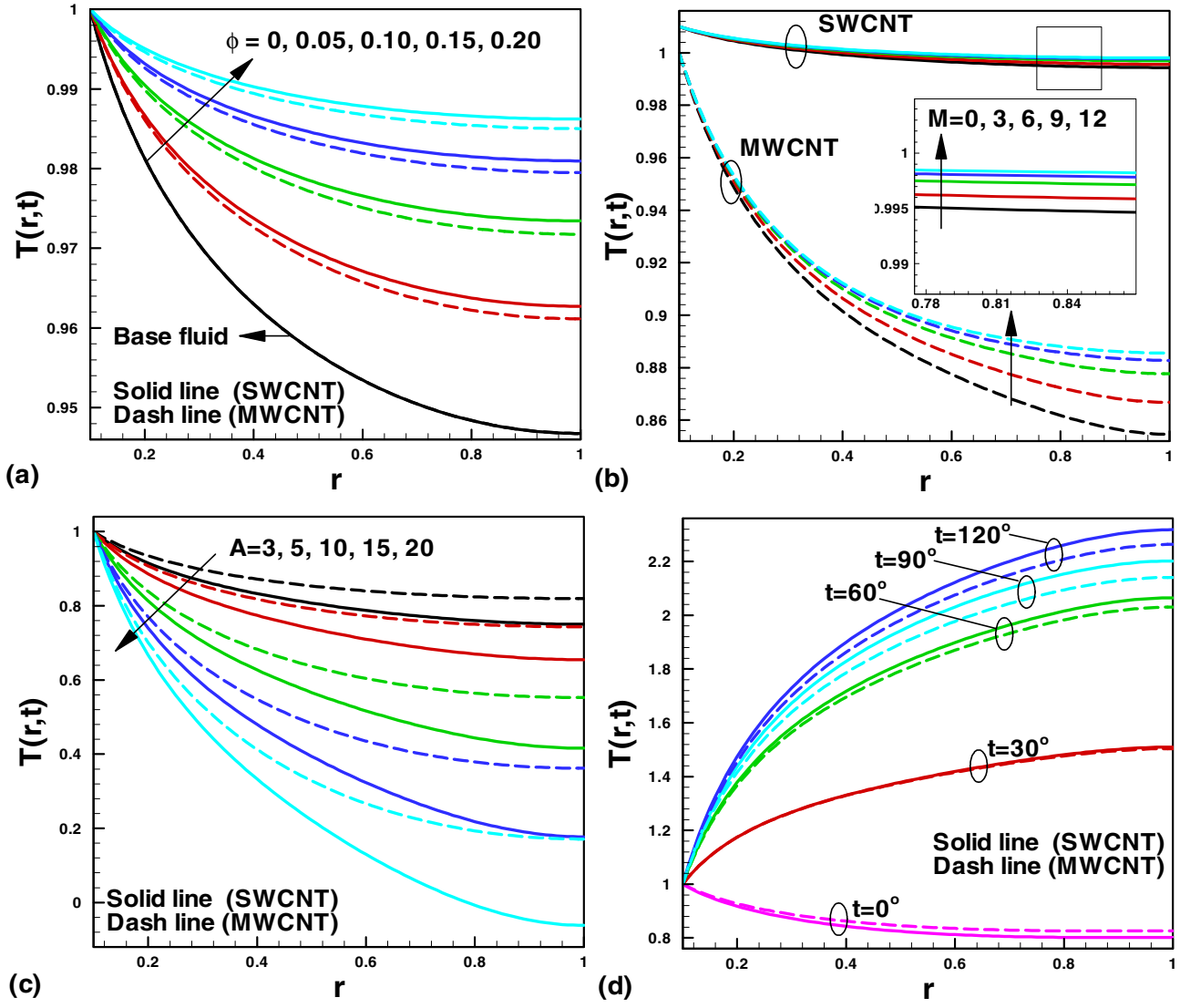


**Fig. 8.** Variation of temperature profile for various values of (a) nanoparticles ($\phi$, (b) Hartmann number $M$, (c) amplitude of pressure gradient $\bar{A}$ and (d) time $t$.

the results obtained for engine-oil based MWCNT (). The decrease in the flow region ends by the increase in velocity, and its miles proven in Fig. 7(a) and (b), where the velocity decreases as nanoparticle volume fraction $\phi$ increases. In Fig. 7(a) and (b) it is noticed that flow area construct set of envelops for various values of radius and velocity field attained maximum position with respect to increasing values of the radius. Since, internal radius of the cylinder remains less or equal to the radius of external cylinder then the domain of the velocity profile restricts $0 \leqslant r \leqslant 1$. Therefore, it may be visible that the velocity attained maximum within the neighborhood of conduits of flow region that changes from 0.7 to 1 and decline in the flow region result in lessen the annular effect. In Fig. 7(b), comparison is made between the engine oil-SWCNT and MWCNT. It is found that engine oil-SWCNT has higher velocity profile as compared to the engine oil-MWCNT.

Examination of heat transferal revolves around the study of temperature profile as well as heat transfer rate situated at the wall. Graphs are plotted to study the effects of nanoparticles $\phi$ Hartmann number $M$, pressure gradient amplitude and time on temperature profile. Fig. 8(a) shows the variation of dimensionless temperature profile for engine oil-based CNTs for varied volume fraction $\phi$. It is spotted that with the increase of nanoparticles

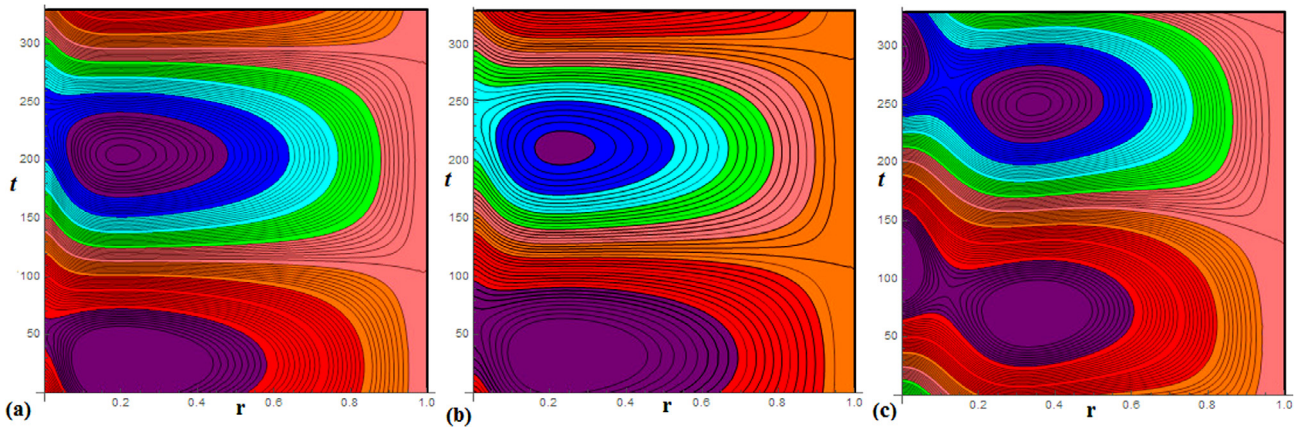


**Fig. 9.** Streamlines for engine oil- based CNTs for (a) base fluid ($\phi = 0$) (b) SWCNT ($\phi = 0.2$) and (c) MWCNT ($\phi = 0.2$).

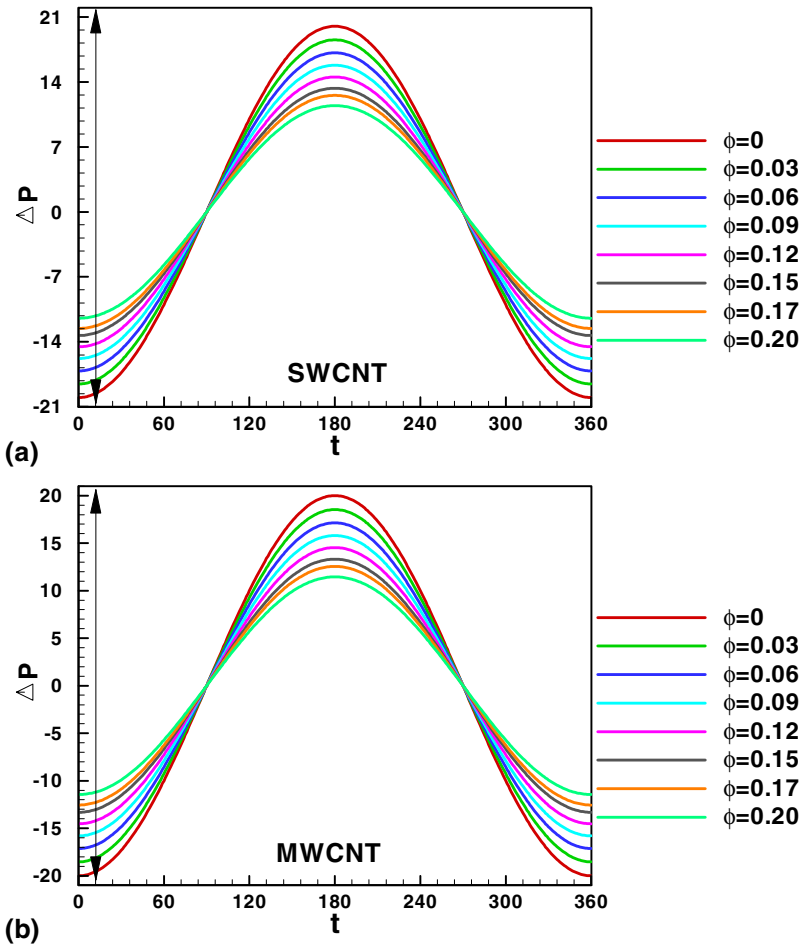


**Fig. 10.** Pressure gradient for (a) SWCNT and (b) MWCNT, when $\bar{A} = 20, M = 10, \alpha = 10$ and $R^* = 0.2$.

enhance the heat transfer profile. Based upon effective thermal conductivity, it is further determined that engine-oil based SWCNTs has higher heat transfer rate as compared to the engine-oil based MWCNTs. However, the base fluid (engine-oil) have low heat transfer rate as compared to the engine-oil based CNTs. Similarly, Fig. 8(b) depicts the variation of temperature profile is plotted against Hartmann number $M$ for both SWCTs and MWCNTs. One can observe that fluid temperature rises due to imposition of the transverse magnetic field. Since magnetic field produces the electric current in fluid which produces heat, then the magnetic field with radiation assists the enhancement phenomena. Fig. 8 (c) and (d) show the effect of pressure gradient amplitude and time on temperature profile. It is found that that increase of pressure gradient amplitude reduces the temperature profile; however, these results are quite opposite for time $t$.

Figs. 9 and 10 shows the variation of stream line and pressure gradient, respectively. In Fig. 9, results are plotted for stream line to analyze the variation of flow behavior for base fluid and engine-oil based CNTs. Similarly, pressure gradient is determined for increasing values of nanoparticle volume fraction (both SWCNTs and MWCNTs). In Fig. 10, it is found that, at the mean position of the duct with $t = 180^{\circ}$, pressure gradient is maximum but attained a decreasing behavior. However, at $t = 0^{\circ}$ and $t = 360^{\circ}$ pressure gradient is minimum but predicts the increasing behavior with respect to the increasing values of nanoparticle volume fraction. It is important to note that in the case of engine-oil based SWCNTs, higher pressure gradient is obtained as compared to the engine-oil based MWCNTs.

## Conclusions

MHD pulsatile flow of carbon nanofluid between two concentric ducts is investigated. Close form solutions are obtained for velocity and temperature distribution with oscillating pressure gradient. The influence of magnetic strength on heat transfer has been studied analytically, that is useful for the potential of blood conduct when confronted with magnetic strength. It could be established that the flow of blood and pressure can be managed sufficiently by the application of an external magnetic field. This will guide to abate some arterial diseases. The solution of velocity, pressure and temperature are demonstrated graphically for a wide ranges of Reynolds number, volume fractions, and Hartmann numbers. In addition, the outcome confirmed that the temperature might be administer by means of the external magnetic and so the heat transfer could possibly be reduced or improved by acquisitive the acuteness of the magnetic field.

- Maximum values of velocity decreases through broaden in the CNTs volume fraction.
- It is also seen that addition of CNTs tremendously increases the temperature of base fluid.
- Nanofluids are robust coolants than natural base fluids as they are able to get rid of extra warmness than average base fluids. So increase in Womersley number leads to reduce the viscous forces gradually because Womersley number is the ratio of pulsation to the viscous forces.
- It is also found that reducing viscos forces enhance the motion of the fluid particles to become faster and consequently velocity profile increase progressively.
- In view of effective thermal conductivity, it is further determined that engine-oil based SWCNTs has higher heat transfer rate as compared to the engine-oil based MWCNTs.

## Acknowledgment

Authors would like to acknowledge and express their gratitude to the United Arab Emirates University, Al Ain, UAE for providing the financial support with Grant No. 31S212-UPAR 9(2015).

## References

[1] Atabek HB, Chang CC. Oscillatory flow near the entry of circular tube. ZAMP 1961;12:405422.
[2] Vardanyan VA. Effect of magnetic field on blood flow. Biofizika 1973;18 (3):491–6.
[3] Richardson EG. Amplitude of sound waves in resonators. Proc Phys Soc London 1928;40(27):206–20.
[4] Richardson EG, Tyler E. Transverse velocity gradient near the mouths of pipes in which an alternating or continuous flow of air is established. Proc R Soc London A 1929;42(1):1–15.
[5] Womersley JR. Method for the calculation of velocity, rate of flow and viscous drag in arteries when the pressure gradient is known. J Physiol 1955;127 (3):553–63.
[6] Uchida S. Pulsating viscous flow superposed on the steady laminar motion of incompressible fluid in a circular pipe. J Appl Math Phys 1956;7(5):403–22.
[7] Yang A, Chen L, Xie Z, Feng H, Sun F. Constructal heat transfer rate maximization for cylindrical pin-fin heat sinks. Appl Therm Eng 2016;108 (5):427–35.
[8] Cui X, Islam MR, Mohan B, Chua KJ. Developing a performance correlation for counter-flow regenerative indirect evaporative heat exchangers with experimental validation. Appl Therm Eng 2016;108(5):774–84.
[9] Dhole AE, Yarasu RB, Lata DB. Effect of hydrogen and producer gas as secondary fuels on combustion parameters of a dual fuel diesel engine. Appl Therm Eng 2016;108(5):764–73.
[10] Tan Q, Hu Y. A study on the combustion and emission performance of diesel engines under different proportions of $O_2$ & $N_2$ & $CO_2$. Appl Therm Eng 2016;108(5):508–15.
[11] Rassoulinejad-Mousavi SM, Seyf Hamid Reza, Abbasbandy S. Heat transfer through a porous saturated channel with permeable walls using two-equation energy model. J Porous Media 2013;16(3):241–54.
[12] Rassoulinejad-Mousavi SM, Abbasbandy Saied. Analysis of forced convection in a circular tube filled with a Darcy-Brinkman-Forchheimer porous medium using spectral homotopy analysis method. ASME J Fluids Eng 2011;133 (10):101207.
[13] Rassoulinejad-Mousavi SM, Porkhial S, Layeghi M, Nikaeen B, Samanipour H. Experimental study on thermal behavior of a stainless steel-di water flat plate heat pipe. World Appl Sci J 2012;16(10):1393–7.
[14] Seyf HR, Rassoulinejad-Mousavi SM. An analytical study for fluid flow in porous media imbedded inside a channel with moving or stationary walls subjected to injection/suction. ASME J Fluids Eng 2011;133(9):091203.
[15] Rassoulinejad-Mousavi SM, Abbasbandy Saied, Alsulami HH. Analytical flow study of a conducting Maxwell fluid through a porous saturated channel at various wall boundary conditions. Eur Phys J Plus 2014;129(181):1–10.
[16] Sanyal DC, Biswas A. Pulsatile motion through an axisymmetric artery in presence of magnetic field. Assam Univ J Sci Technol Phys Sci Technol 2010;5 (2):12–20.
[17] Yakhot A, Grinberg L. Phase shift ellipses for pulsating flows. Phys Fluids 2003;15(7):132–8.
[18] Suces J. An improved quasi-study approach for transient conjugated forced convection problems. Int J Heat Mass Transfer 1981;24(10):711–1722.
[19] Latham TW. Fluid motions in a peristaltic pump. Massachusetts Inst Technol 1966:72–4.
[20] Majdalani J. Pulsatory Channel Flows with Arbitrary Pressure Gradients, AIAA.3rd: Theoretical Fluid Mechanics Meeting, 2002. p. 24–26.
[21] Agrawal HL, Anwaruddin B. Peristalic flow of blood in a branch. Ranchi Univ Math J 1984;15:111–21.
[22] Tzirtzilakis EE. A mathematical model for blood flow in magnetic field. Phys Fluids 2005;17(7):077103–15.
[23] Ramamurthy G, Shanker B. Magneto hydrodynamic effects on blood flow through porous channel. Med Biol Eng Comput 1994;32(6):655–9.
[24] Choi SUS. Enhancing thermal conductivity of fluids with nanoparticles, developments and applications of non-Newtonian flows. ASME FED 1995;231:99–103.
[25] Choi SUS. Nanofluids from vision to reality through research. J Heat Transfer 2009;131:1–9.
[26] Yu W, France DM, Routbort JL, Choi SUS. Review and comparison of nanofluid thermal conductivity and heat transfer enhancements. Heat Transfer Eng 2008;29:432–60.
[27] Das SK, Choi SUS, Patel HE. Heat transfer in nanofluids a review. Heat Transfer Eng 2006;27:3–9.
[28] Liu MS, Lin MCC, Huang IT, Wang CC. Enhancement of thermal conductivity with carbon nanotube for nanofluids. Int Commun Heat Mass Transfer 2005;32:1202–10.
[29] Buongiorno J. Convective transport in nanofluids. J Heat Transfer 2005;128 (3):240–50.

[30] Akbar NS, Nadeem S. Mixed convective magnetohydrodynamic peristaltic flow of a Jeffrey nanofluid with Newtonian heating. Z Naturforsch 2013;68:433–41.
[31] Emad AH, Ebaid A. New exact solutions for boundary-layer flow of a nanofluid past a stretching sheet. J Comput Theor Nanosci 2013;10:2591–4.
[32] Liu Z, Liu Y, Chang Y, Seyf HR, Henry A, Matteyses AL, Yehl K, Zhang Y, Huang Z, Salaita K. Nanoscale optomechanical actuators for controlling mechanotransduction in living cells. Nat Methods 2016;13(2):143–6.
[33] Rassoulinejad-Mousavi SM, Mao Y, Zhang Y. Evaluation of copper, aluminum, and nickel interatomic potentials on predicting the elastic properties. J Appl Phys 2016;119(24):244304.
[34] Shalchi-Tabrizi A, Seyf HR. Analysis of entropy generation and convective heat transfer of $Al_2O_3$ nanofluid flow in a tangential micro heat sink. Int J Heat Mass Transfer 2012;55(15–16):4366–75.
[35] Seyf HR, Nikaaein B. Analysis of Brownian motion and particle size effects on the thermal behavior and cooling performance of microchannel heat sinks. Int J Therm Sci 2012;58:36–44.
[36] Seyf HR, Feizbakhshi M. Computational analysis of nanofluid effects on convective heat transfer enhancement of micro-pin-fin heat sinks. Int J Therm Sci 2012;58:168–79.
[37] Hussain ST, Ul Haq Rizwan, Khan ZH, Nadeem S. Water driven flow of carbon nanofluid nanotubes in a rotating channel. J Mol Liq 2016;214:136–44.
[38] Ul Haq Rizwan, Hussain ST, Khan ZH, Hammouch Z. Flow and heat transfer analysis of water and ethylene glycol based *Cu* nanoparticles between two parallel disks with suction/injection effects. J Mol Liq 2016;221:298–304.
[39] Atlas M, Ul Haq Rizwan, Mekkaoui T. Active and zero flux of nanoparticles between a squeezing channel with thermal radiation effects. J Mol Liq 2016;223:289–98.
[40] Hussain ST, Nadeem S, Ul Haq Rizwan. Model based analysis of micropolar nanofluid flow over a stretching surface. Eur Phys J Plus 2014;129:167.
[41] Ijima S. Helical microtubules of graphitic carbon. Nature 1991;354:56–8.
[42] Cheng Y, Zhou O. Electron field emission from carbon nanotubes. C R Phys 2003;4:1021–33.
[43] Timofeeva EV, Routbort JL, Singh D. Particle shape effects on thermo- physical properties of alumina nanofluids. J Appl Phys 2009;106(1):014304–10.
[44] Sohel Murshed SM, Nietode Castro CA, Lourenço MJV, Lopes MLM, Santos FJV. A review of boiling and convective heat transfer with nanofluids. Renewable Sustainable Energy Rev 2011;15(5):2342–54.